Communication

Effect of Hydrogen Doping on Stress-Induced Martensitic Transformation in a Ti-Ni Shape Memory Alloy

ZHENXING LI, FEI XIAO, XIAO LIANG, HONG CHEN, ZHU LI, XUEJUN JIN, and TAKASHI FUKUDA

In this paper, we report how the charged hydrogen in a Ti-50.8Ni (at. pct) alloy acts during stress-induced martensitic transformation and aging. Hydrogen is preferentially trapped in the B19′ martensite phase near the surface of the specimen. The hydride formed by hydrogenation dissociates during the stress-induced martensitic transformation. The hydrogen diffuses into the interior of the specimen through aging in air, resulting in suppression on the stress-induced martensitic transformation.

https://doi.org/10.1007/s11661-019-05258-1

Ti-Ni shape memory alloys (SMAs) are widely used in commercial products due to their unique superelastic property.[1–4] This property depends on the stress-induced austenite-to-martensite phase transformation in Ti-Ni SMAs.[1–6] It has been pointed out by many researchers that the phase transformation and mechanical behaviors of Ti-Ni SMAs could be significantly affected by hydrogen absorption.[7–13] Since hydrogen atoms can inadvertently enter Ti-Ni SMAs through electrolysis, pickling, or other means in a hydrogen-containing environment, the interaction of hydrogen with Ti-Ni SMAs is a key concern in the performance of the material.

Several studies have revealed the effect of hydrogen on the thermal-induced martensitic transformation (MT) of Ti-Ni SMAs.[14–16] It is commonly agreed that the thermal-induced MT of Ti-Ni SMAs is suppressed by hydrogen charging. The transformation temperature decreases and the latent heat reduces.[14,15] The reason for the suppression was explained by the trapped hydrogen, which acts as a barrier so as to block the progress of MT. This blocking effect of hydrogen possibly affects the progress of stress-induced MT as well. In fact, it is found in a hydrogen-charged Ti-Ni alloy that the critical stress for inducing MT increases and fracture occurs during the stress-induced MT. Considering these results, Runciman *et al*. affirmed that hydrogen stabilizes the austenite phase and suppresses the MT.[14] However, a recent research showed that hydrogen ensures the stability of the phase in which the charging process occurs, rather than the austenite phase.[17] Therefore, the mechanism of the effect of hydrogen on the stress-induced MT is still unclear. Moreover, no report has been made on the *in situ* structural evolution during the stress-induced MT of hydrogen-charged Ti-Ni SMAs.

In this study, we examined the influence of hydrogen on stress-induced MT in a Ti-50.8Ni (at. pct) alloy by *in situ* X-ray analysis. In addition, we observed the diffusion of hydrogen into the interior of specimen during the aging process by SEM-TOF-SIMS.

A hot-rolled Ti-50.8Ni (at. pct) sheet with the thickness of 2 mm was purchased from Fasten-PLT Materials Science Co., Ltd. In this study, we employed a cold-rolling treatment to enhance the fatigue behavior of the Ti-Ni SMAs.[18] After being cold rolled to 50 pct thickness reduction (final thickness ~ 1 mm), tensile test specimens with dimensions of 20 mm in gage length, 3 mm in width, and 1 mm in thickness were cut along the rolled direction by means of slow wire-electrode cutting method. The specimens were then annealed at 673 K for 1 hour.

The cathodic hydrogen charging of the samples was carried out by immersion in an aqueous 0.9 pct NaCl solution at 10 A/m^2 for 1 hour at room temperature (RT). Anode material is a platinum wire. We term the specimen without hydrogen charging as NC, charged specimen as C10, and C10 sample after aging for n hours at RT as C10-Anh.

The transformation characteristics of these samples were measured using a Differential Scanning Calorimeter (DSC) NETZSCH model 200F3 in temperatures ranging from 123 K to 423 K at a cooling/heating rate of 10 K/min, and standard four-point contact electrical resistivity (ER) measurements in temperatures ranging from 10 K to 400 K at a cooling/heating rate of 2 K/min.

ZHENXING LI, XIAO LIANG, HONG CHEN, and ZHU LI are with the State Key Lab of Metal Matrix Composite, School of Materials Science and Engineering, Shanghai Jiao Tong University, 800 Dong Chuan Road, Shanghai 200240, P.R. China. FEI XIAO is with the State Key Lab of Metal Matrix Composite, School of Materials Science and Engineering, Shanghai Jiao Tong University and also with the Department of Materials Science and Engineering, Graduate School of Engineering, Osaka University, 2-1, Yamada-oka, Suita, Osaka 565-0871, Japan. Contact e-mail: xfei@sjtu.edu.cn XUEJUN JIN is with the Institute of Advanced Steels and Materials, School of Materials Science and Engineering, Shanghai Jiao Tong University, Shanghai 200240, P.R. China. TAKASHI FUKUDA is with the Department of Materials Science and Engineering, Graduate School of Engineering, Osaka University

Manuscript submitted November 20, 2018.
Article published online May 14, 2019

The uniaxial tensile experiments were performed on Instron-5966 mechanical testing machine at a loading/unloading strain rate of 5×10^{-3} s^{-1} at RT. The structural evolution under the tensile strain was monitored using a Bruker D8 Advance XRD, with Cu-K_α radiation. The hydrogen-charged specimens after aging in air at RT for different times were also investigated by XRD. Vickers microhardness tests have also been performed under an applied load of 9.8 N for 10 seconds. The distribution of hydrogen is detected by means of SEM equipped with Time of Flight Secondary Ion Mass Spectrometry (TOF-SIMS).

Figure 1(a) shows the DSC heat flow for the NC and C10 samples. In the cooling process, two separated exothermic peaks appear for both the specimens. They correspond to the B2 $\rightarrow$ R and R $\rightarrow$ B19′ transformations, respectively. In the heating process, however, the endothermic peaks of the B19′ $\rightarrow$ R and R $\rightarrow$ B2 transformations are not separated for both the specimens. The absolute value s of the latent heats (ΔH) calculated by integrating the peak area are summarized in Table I. It is found that the $|\Delta H|$ decreases after charging, especially for the successive B19′ $\rightarrow$ R $\rightarrow$ B2 transformation. This result suggests that the volume of the alloy undergoing phase transformation decreases by hydrogen doping.

We also performed ER measurements to confirm the transformation behavior. The temperature dependences of ER ρ for the NC and C10 specimens are shown in Figure 1(b). The increase in resistivity in the cooling process is due to the B2 $\rightarrow$ R MT, and the subsequent decrease is due to the R $\rightarrow$ B19′ MT. The change in slope in the heating process is due to B19′ $\rightarrow$ R MT, and the subsequent decrease is due to R $\rightarrow$ B2 MT. The differences in ER between heating and cooling processes at the highest peak position $\Delta\rho$ (Figure 1(b)) are summarized in Table I. It is found that the $\Delta\rho$ decreases obviously after hydrogen charging. This result again suggests that the amount of B19′ martensite formed by the thermal-induced MT decreased by hydrogenation. The MT temperatures (M_{Rs}: start temperature of B2 $\rightarrow$ R MT, M_s: start temperature of R $\rightarrow$ B19′ MT, M_f: finish temperature of R $\rightarrow$ B19′ MT, A_s: start temperature of B19′ $\rightarrow$ R transformation, A_{Rs}: start temperature of R $\rightarrow$ B2 transformation, A_f: finish temperature of R $\rightarrow$ B2 transformation) are indicated in the figure, and the results are shown in Table I. We notice that the change in transformation temperatures by hydrogen doping is small.

In order to investigate the influence of the hydrogen on the mechanical behavior, tensile tests for the hydrogen-charged and noncharged specimens were conducted. Figure 1(c) shows the stress–strain curves for the NC (black) and C10 (red) specimens at 338 K (both above A_f). Both specimens show a change in slope, which should be caused by the stress-induced B2$\rightarrow$R transformation, followed by a plateau characteristic to R $\rightarrow$ B19′ MT. There is almost no change in B2-R phase transition after hydrogen charging. However, hydrogen charging causes an obvious increase in the plateau characteristic to R $\rightarrow$ B19′ MT. By employing the tangent method, the critical stress for inducing MT (σ_c) was determined to be 201 MPa for the NC specimen and 225 MPa for the C10 specimen. The increase of σ_c by hydrogen doping is consistent with previous reports.[19,20] This result suggests that hydrogen suppresses the stress-induced MT. Since A_f is higher than RT, there is residual strain after removing the stress.

The increase in σ_c implies that the slope ($d\sigma/dT$) of the phase boundary increases by hydrogen doping. Then from the Clapeyron equation, we know that $|\Delta S/\Delta\varepsilon|$ increases by hydrogen charge, where ΔS is the entropy change of transformation and $\Delta\varepsilon$ is the transformation strain.[21]

In order to study the structural evolution during the tensile process, an *in situ* XRD test was performed. Figure 2 shows the diffraction profiles of the NC and C10 samples measured under different tensile strains during the loading and the subsequent unloading processes at 295 K. Before the measurements, the specimen was cooled from 350 K. For the NC sample without strain, the specimen is composed mainly of parent B2-phase (110_{B2}), and R-phase (112_R, 300_R) including a small amount of B19′-phase ($101_{B19'}$), which is probably induced by cold-rolling treatment. As the strain increases to about 2 pct, the B2-phase and the R-phase transform to the B19′-phase. Upon further increasing the strain, the B2 reflection (110_{B2}) continuously decreases, and the B19′ reflections ($110_{B19'}$ and $020_{B19'}$) grow. In the subsequent unloading process, the B19′ martensite phase transforms back to the B2 parent phase. Since A_f is higher than RT, there is residual strain after removing the stress, and the stress-induced martensite phase could not be fully converted back to the parent phase.

The X-ray profile of the hydrogen-charged (C10) sample also includes peaks of B2, R, and B19′ phases as the NC specimen. The main difference is that it includes peaks of the hydride TiNiH (tetragonal; a = 0.6221 nm, c = 1.2363 nm).[22,23] The position of the $101_{B19'}$ reflection slightly shifts to a lower angle compared with the NC specimen. This implies the increase in the lattice constant $d(101)$ of the B19′-phase due to interstitial hydrogen atoms.[24] However, the initial position for the 110_{B2} reflection of the C10 specimen is almost the same as that of the NC specimen, where the difference in

Table I. The Entropy Changes of Phase Transformation, Transformation Temperatures, and $\Delta\rho$ for NC and C10 Specimens

	$\lvert\Delta H\rvert$ (kJ/mol)				Transformation temperature (K)					
Specimens	B2 $\rightarrow$ R	R $\rightarrow$ B19′	B19′ $\rightarrow$ R $\rightarrow$ B2	$\Delta\rho$ ($\mu\Omega$ cm)	M_{Rs}	M_s	M_f	A_s	A_{Rs}	A_f
NC	0.35	0.35	0.97	0.23	323	265	202	283	315	327
C10	0.33	0.31	0.89	0.15	323	267	204	290	314	324

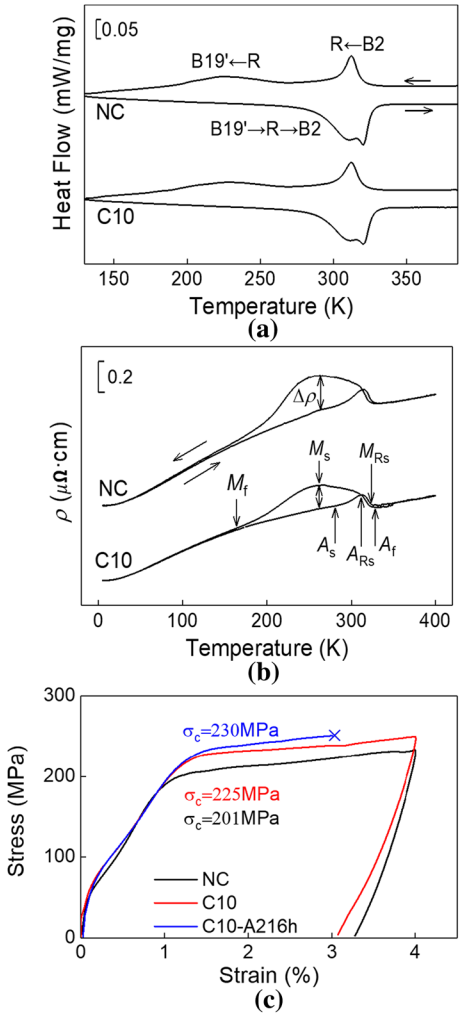

Fig. 1—(*a*) DSC and (*b*) electrical resistivity cooling and heating curves of the Ti-50.8Ni (at. pct) NC and C10 specimens. The transformation temperatures A_s, A_f, M_s, M_f, A_{Rs}, M_{Rs}, and $\Delta\rho$ are indicated. (*c*) Stress–strain curves for the Ti-50.8Ni (at. pct) NC (black), C10 (red), and C10 after aging for 216-h (blue) specimens at RT. The critical stresses for inducing martensitic transformation are indicated (Color figure online).

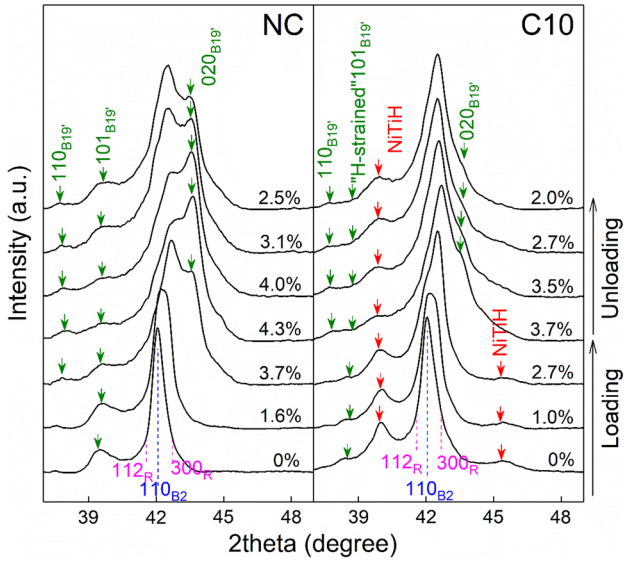

Fig. 2—*In situ* X-ray diffraction profiles under different tensile strains of the Ti-50.8Ni (at. pct) NC and C10 specimens during the loading and unloading processes at RT.

lattice constants is within 0.02 pct. This means that hydrogen is preferentially trapped in the B19′ martensite phase. This speculation is supported by a previous report which demonstrates that hydrogen readily moves from sites in the parent phase to sites in the martensite phase because the hydrogen solubility and diffusivity in the martensite phase of the alloy are larger than those in the parent phase.[25–27] Therefore, this behavior suggests that two distinct B19′ structures coexist in the sample: one is "unstrained" B19′ phase which exists in most parts of the specimen; and the other is "hydrogen-strained" B19′-phase which exists in the vicinity of the surface.

As the strain of the C10 specimen increases, the B2-phase and R-phase transform into the B19′ martensite structure. Notice that the stress-induced B19′ martensite phase peak of the NC sample under the same strain is obviously larger than that in the C10 sample, so the fraction of the formed B19′ martensite phase in the hydrogen-filled sample is less than that of the uncharged sample, which confirms the suppression of MT by hydrogen doping. A remarkable result is that the hydride reflection gradually shrinks during the loading process, which implies that hydride gradually dissociated during the stress-induced MT.

According to a report by Tomita *et al.*, the charged hydrogen initially exists in the vicinity of the surface of the sample, and gradually diffuses toward the center of the sample during aging in air environment.[20] This implies that aging affects the stress-induced transformation behavior and structural evolution of the Ti-Ni alloy. To understand the effect of aging, the hydrogen-charged sample was examined after aging. Figure 3 shows the XRD evolution of the C10 sample during aging at RT in air (black curves), and the results were compared with the NC sample (blue curve). As the aging duration increases, the intensity of the reflection of the hydride gradually decreases, and the "hydrogen-strained" $101_{B19'}$ reflection shifts back to higher angle. After aging for about 9 days, the hydride almost completely dissociates, and the "hydrogen-strained" $101_{B19'}$ reflection returns back to its original position. It is found that the diffraction pattern is almost the same as that for the NC specimen.

In order to know the influence of diffused hydrogen, the tensile behavior was tested on the C10 sample after aging 9 days at RT, and the results are shown in Figure 1(c) (blue curve). It is found that σ_c further increases to 230 MPa, and the specimen fractures in the stress-induced transformation plateau stage. This result implies that it is hydrogen in solid solution rather than hydride that deteriorates the mechanical properties of Ti-Ni SMAs.

To confirm the diffusion of hydrogen in Ti–Ni SMA, hardness of the specimen was examined as a function of

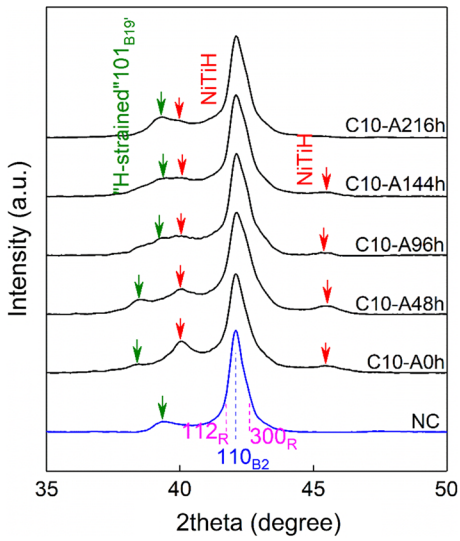

Fig. 3—X-rays diffraction profiles of the Ti-50.8Ni (at. pct) NC (blue curve) and C10 (black curve) specimens during aging at RT in air environment (Color figure online).

the distance from the surface for the C10 and aged specimens, and the results were compared then to those of the NC specimen (Figure 4(a)). The microhardness of the NC specimen (black) is approximately 298 Hv throughout the specimen. A significant hardening in the vicinity of the surface can be seen for the C10 specimen (red). The hardness is about 325 Hv near the surface and decreases progressively to the value of the NC specimen. This implies that the center of C10 specimen is almost unaffected by hydrogen charging. However, after 48 h of aging (blue), the hardness decreases to 313 Hv near the surface of the specimen, but the hardness is higher than that of the C10 specimen when the distance from the surface exceeds 0.1 mm. This result confirms that the hydrogen diffuses from the surface toward the center during aging and affects the whole specimen.

In order to confirm the distribution of hydrogen elements, time-of-flight secondary ion mass spectrometry (TOF-SIMS) was conducted for the C10 and C10-A48h specimens. The specimens were stretched until fractured, and the fracture surfaces were examined by SEM-TOF-SIMS. The color in Figure 4(b) indicates the relative concentration of hydrogen. In the C10 specimen (a), most of hydrogen exist in the vicinity of surface; the hydrogen enrichment depth is ~ 100 μm, which is consistent with the result of hardness test. In the C10-A48h specimen, we notice that hydrogen is distributed to ~ 300 μm from the surface although it is still enriched near the surface. This result clearly indicates that hydrogen diffuse into the interior of the specimen during aging.

From the above results, we speculate that hydrogen suppresses both the thermal- and stress-induced martensitic transformations and most of hydrogen exists in the vicinity of the surface of the sample immediately after charging. Hydrogen is preferentially trapped in the B19′ martensite phase due to the higher hydrogen solubility

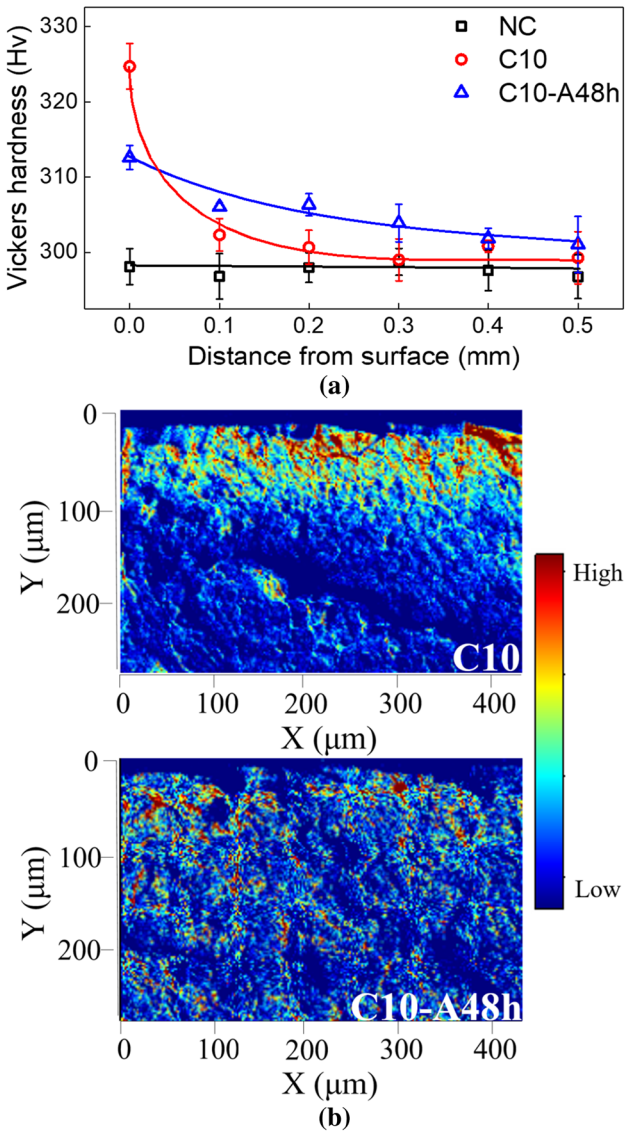

Fig. 4—(*a*) Vickers microhardness depth profiles of the NC (black), C10 (red), and C10 after aging for 48 h (blue). (*b*) Distribution of hydrogen in the cross sections of the C10 and C10-A48h. The top is the surface of the specimen (Color figure online).

and diffusivity in the martensite phase. Hydrogen at the surface layer of the specimen gradually diffuses into the center of the specimen during aging process. Therefore, σ_c further increases and specimen fractures early after the aging process. Meanwhile, due to the diffusion of the hydrogen from the B19′ martensite phase near the surface into interior of specimen, the "hydrogen-strained" $101_{B19'}$ reflection can return back to its original position during aging process. In addition, hydride forms immediately after hydrogen charging and dissociates during aging in air.

In this paper, effects of hydrogen on the stress-induced MT of the Ti-50.8Ni (at. pct) SMA were investigated. The hydrogen suppresses both the thermal- and stress-induced martensitic transformations, where the latent heat caused by the MT decreased and the critical

stress for inducing MT increased. The *in situ* structural evolution confirmed that hydrogen preferentially undergoes trapping in the B19′ martensite phase near the surface of the specimen. Hydride formed immediately after hydrogen charging and dissociated during the stress-induced MT. After a long-time aging at RT in the air environment, the critical stress further increased, and the specimen fractured during the stress-induced martensitic transformation due to the diffusion of hydrogen into interior of the specimen.

This work was funded by the National Natural Science Foundation of China (Nos. 51871151, 51501113, U1564203), the National Key R&D Program of China (Nos. 2017YFB0703003, 2017YFB0406000), and the Iketani Science and Technology Foundation (No. 0301012-A).

REFERENCES

1. K. Otsuka and X. Ren: *Prog. Mater. Sci*, 2005, vol. 50, pp. 511–678.
2. T. Duerig, A. Pelton, and D. Stockel: *Mater. Sci. Eng. A*, 1999, vols. 273–275, pp. 149–60.
3. F. Xiao, H. Chen, X. Jin, Z. Nie, T. Kakeshita, and T. Fukuda: *Sci. Rep*, 2018, vol. 8, p. 6099.
4. X. Liang, F. Xiao, M. Jin, X. Jin, T. Fukuda, and T. Kakeshita: *Scripta Mater*, 2017, vol. 134, pp. 42–46.
5. J.M. Jani, M. Leary, A. Subic, and M.A. Gibson: *Mater. Des*, 2014, vol. 56, pp. 1078–1113.
6. F. Xiao, T. Fukuda, and T. Kakeshita: *Scripta Mater*, 2016, vol. 124, pp. 133–37.
7. K. Yokoyama, K. Hamada, K. Moriyama, and K. Asaoka: *Biomaterials*, 2001, vol. 22, pp. 2257–62.
8. N. Wade, Y. Adachi, and Y. Hosoi: *Scripta Mater*, 1990, vol. 24, pp. 1051–55.
9. K. Yokoyama, S. Watabe, K. Hamada, J. Sakai, K. Asaoka, and M. Nagumo: *Mater. Sci. Eng. A*, 2003, vol. 341, pp. 91–97.
10. K. Yokoyama, K. Kaneko, K. Moriyama, K. Asaoka, J. Sakai, and M. Nagumo: *J. Biomed. Mater. Res*, 2003, vol. 65A, pp. 182–87.
11. K. Yokoyama, T. Ogawa, K. Asaoka, J. Sakai, and M. Nagumo: *Mater. Sci. Eng. A*, 2003, vol. 360, pp. 153–59.
12. K. Yokoyama, M. Tomita, and J. Sakai: *Acta Mater*, 2009, vol. 57, pp. 1875–85.
13. A. Biscarini, R. Campanella, B. Coluzzi, G. Mazzolai, L. Trotta, A. Tuissi, and F.M. Mazzolai: *Acta Mater*, 1999, vol. 47, pp. 4525–33.
14. A. Runciman, K.C. Chen, A.R. Pelton and C. Trépanier: SMST-2006 Proc. Int. Conf. on Shape Memory and Superelastic Technologies, Pacifi Grove, CA, USA, 2006, pp. 185–196, https://doi.org/10.1361/cp2006smst185.
15. M. Kuběnová, J. Zálešák, J. Čermák, and A. Dlouhý: *J. Alloy. Compd*, 2013, vol. 577S, pp. S287–S290.
16. Y. Snir, M. Carl, N.A. Ley, and M.L. Young: *Shap. Mem. Superelast.*, 2017, vol. 3, pp. 443–56.
17. E. Letaief, T. Hassine, and F. Gamaoun: *Mater. Sci. Technol.*, 2017, vol. 33 (13), pp. 1533–38.
18. H. Yin, Y. He, Z. Moumni, and Q. Sun: *Int. J. Fatigue*, 2016, vol. 88, pp. 166–77.
19. F. Gamaoun, M. Ltaief, T. Bouraoui, and T.B. Zineb: *J. Intell. Mater. Syst. Struct*, 2011, vol. 22, pp. 2053–59.
20. M. Tomita, K. Yokoyama, K. Asaoka, and J. Sakai: *Mater. Sci. Eng. A*, 2008, vol. 476, pp. 308–15.
21. E. Bonnot, R. Romero, L. Manosa, E. Vives, and A. Planes: *Phys. Rev. Lett*, 2008, vol. 100, p. 125901.
22. D. Noéus, P.-E. Werner, K. Alasafi, and E. Schmidt-Ihn: *Int. J. Hydrogen Energy*, 1985, vol. 10, pp. 547–50.
23. J.L. Soubeyroux, D. Fruchart, G. Lorthioir, P. Ochin, and D. Colin: *J. Alloys. Compd.*, 1993, vol. 196, pp. 127–32.
24. T. Ohba, F. Yanagita, M. Mitsuka, T. Hara, and K. Kato: *Mater. Trans.*, 2002, vol. 43, pp. 798–801.
25. R. Burch and N.B. Mason: *J. Chem. Soc. Faraday Trans.*, 1979, vol. 75, pp. 561–77.
26. F. Cuevas, M. Latroche, P. Ochin, A. Dezellus, J.F. Fernández, C. Sánchez, and A. Percheron-Guégan: *J. Alloys Compd*, 2002, vols. 330–332, pp. 250–55.
27. K. Yokoyama, S. Watabe, K. Hamada, J. Sakai, K. Asaoka, and M. Nagumo: *Mater. Sci. Eng. A*, 2003, vol. 341 (1–2), pp. 91–97.